Voltage-gating of aquaporins, a putative conserved safety mechanism during ionic stresses

Robin Mom, Beatriz Muries, Pierrick Benoit, Julien Robert-Paganin, Stéphane Réty, Jean-stéphane Venisse, Agílio Pádua, Philippe Label, Daniel Auguin

DR. DANIEL AUGUIN (Orcid ID : 0000-0003-4713-9096)

Received Date : 16-Sep-2020

Accepted Date : 19-Sep-2020

Article type : Research Articles

Title:

Voltage-gating of aquaporins, a putative conserved safety mechanism during ionic stresses

Author names:

Robin Mom[1,*], Beatriz Muries[1], Pierrick Benoit[1], Julien Robert-Paganin[2], Stéphane Réty[3], Jean-Stéphane Venisse[1,*], Agilio Padua[4], Philippe Label[1], Daniel Auguin[5,*]

Affiliations:

[1] - UCA, INRA, UMR PIAF, F-63000, Clermont-Ferrand, France

[2]- Structural Motility, Institut Curie, Paris Université Sciences et Lettres, Sorbonne Université, CNRS UMR144, 75005 Paris, France

[3]- Laboratoire de Biologie et Modélisation de la Cellule, ENS de Lyon, University Claude Bernard, CNRS UMR 5239, INSERM U1210, 46 Allée d'Italie Site Jacques Monod, F-69007, Lyon, France.

[4] - Laboratoire de Chimie, ENS de Lyon, Université de Lyon, CNRS, 69364 Lyon, France.

[5] - Université d'Orléans, Laboratoire de Biologie des Ligneux et des Grandes Cultures, UPRES EA 1207, INRAE-USC1328, F-45067, Orléans, France

Corresponding authors : auguin@univ-orleans.fr, robin.mom@uca.fr, j-stephane.venisse@uca.fr

Telephone : +33 2 38 49 48 08

Abstract:

Aquaporins are transmembrane water channels found in almost every living organism. Numerous studies have brought a good understanding of both water transport through their pores and the regulations taking place at the molecular level, but subtleties remain to be clarified. Recently a voltage-related gating-mechanism involving the conserved arginine of the channel's main constriction was captured for human aquaporins through molecular dynamics studies. With a similar approach, we show that this voltage-gating could be conserved among this family and that the underlying mechanism could explain part of plant AQPs diversity when contextualized to high ionic concentrations provoked by drought. Finally we identified residues as adaptive traits which constitute good targets for drought resistance plant breeding research.

Graphical Abstract:

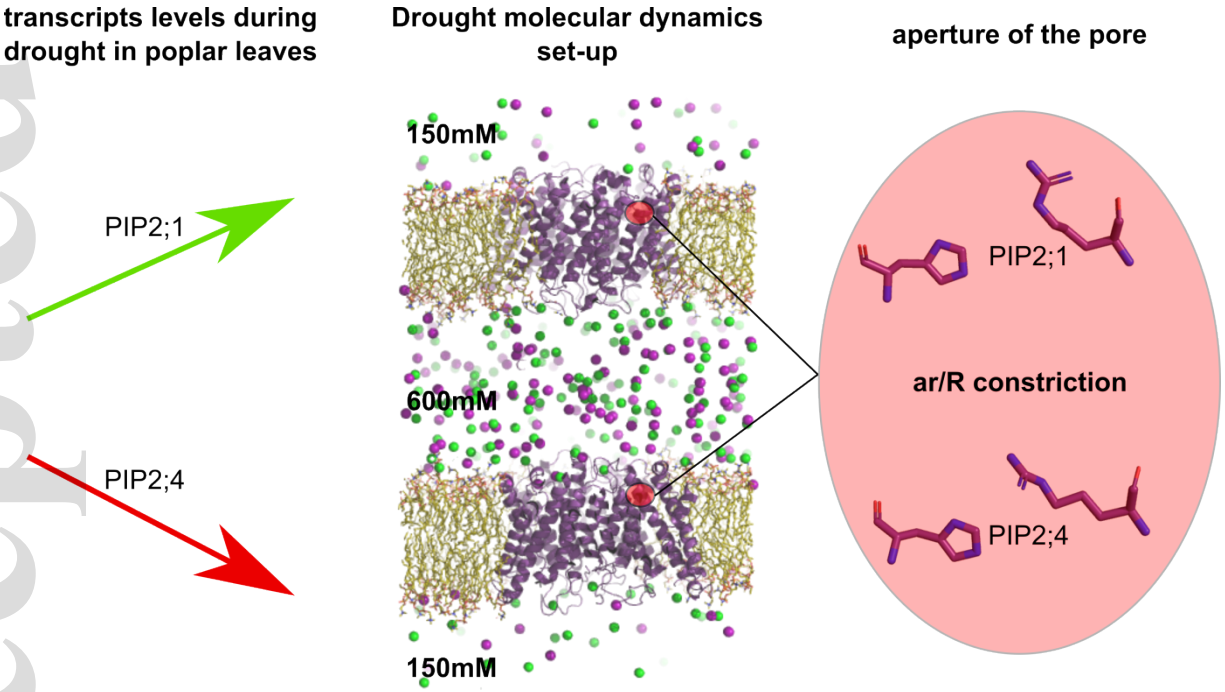

Keywords : Water-Channel, gating, membrane permeability, drought stress, Molecular Dynamics.

Abbreviations :

AQP : Aquaporin

PIP : Plasma membrane Intrinsic Protein

GLP : Glycerol facilitation-Like Proteins

TIP : Tonoplast membrane Intrinsic Protein

MIP : Major Intrinsic Protein

NPA : Asparagine-Proline-Alanine motif

ar/R : Aromatic/Arginine

pf : peameability factor

dRH : Arginine Histidine distance

dRI : Arginine Isoleucine distance

Dk : Diffusion correction parameter

Highlights:

- Diversity in the response of aquaporins toward high membrane potentials.
- Free-energy profiles based correction of *pf*.
- AQPs water permeability tuning through ar/R constriction arginine side-chain conformational changes.
- Phenotypic diversity linked to highly variable extra-cellular loops in plant AQPs.

Introduction

Water is essential for any living organism as it plays a crucial role in metabolism and regulation of cells homeostasis. It can diffuse passively through the plasma membranes of cells but, because of the lipidic nature of the membrane, the rate of diffusion is limited. The discovery of water specific channel proteins initially named major intrinsic proteins (MIPs) and later aquaporins (AQPs) [1] challenged significantly the concepts by which living beings regulate water homeostasis from a subcellular scale to a cell scale and from a cell up to the whole organism scale (for pluricellular organisms). The crucial role of AQPs in cells well-function can be appreciated by their presence in all life forms[2].

While most bacteria and archaea have only two AQPs in their genomes (one AQP and one aquaglyceroporin, GLP, *i.e.* a sub-group of the AQP family able to transport glycerol as well), in eukaryotes gene duplications expanded greatly the diversity of this protein family[2] notably in plants where it can reach hundreds of copies (121 in Brassica napus [3]). This multiplicity can be partly explained by sub-functionalization events. Indeed, in plants AQPs are partitioned between several sub-families according, among other criteria, to their sub-cellular localization: Plasma membrane Intrinsic Proteins (PIPs), Tonoplast Intrinsic Proteins (TIPs). Neo-functionalization events also occurred, leading to both selectivity toward different solutes (on top of water) such as glycerol[4] or other small molecules[5], and the apparition or sophistication of gating mechanisms [6].

Aquaporins are naturally found as tetramers[7]. Each subunit consists of six transmembrane helices. The helices are organized symmetrically in two funnel-shaped vestibules and the conduction pore is formed in their center: it is the so-called hourglass structure of the AQPs [8]. Within the channel, the permeation is ensured by a succession of polar interactions between the solute molecules and aminoacids of the AQP. Two main constriction sites are involved in the selectivity of the pore. The very conserved NPA motifs with the two asparagine side-chains pointing out into the pore are located at the end of two half helices, which through their dipoles generate an electrostatic barrier in this region essential for proton exclusion[9] . The aromatic residue/arginine (ar/R) constriction, which constitutes the narrowest part of the pore is believed to

be determinant in substrate selectivity of the channel[10][11][4]. The surrounding residues in this region may differ, influencing its size and hydrophobicity[4].

Plants have to cope with constantly changing hydric environment. The variable amplitudes in water availability in time give a tangible explanation of the large diversity for AQPs in their genomes. For instance, the tree model genus *Populus* has an extensive distribution range spanning entire continents for some species and hence is naturally exposed to fluctuating water availability[12], and contains 54 AQP genes. Among these 54 isoforms, 15 belong to the plasmalemmic PIP sub-family with 10 PIP2 and 5 PIP1[13]. In poplar leaves undergoing drought, 11 of these PIP genes are differentially expressed[14]. All are so-called strict AQPs, meaning that they all possess the same characteristic ar/R constriction (F81-H210-T219-R225 in the reference structure of *So*PIP2;1[6]) allowing small polar solutes (*i.e.* water) only to commute through the pore (figure 1a). Beyond the selectivity of the channel, its activity can be modulated through gating mechanisms. In plant AQPs, one of them have been described thoroughly and involves pH, cations and the placement of intra-cellular D-loop[6]. The residues implicated in the closing of the pore are strictly conserved among poplar PIPs (figure 1b). We could question this apparent functional redundancy, as the structural features mentioned above are involved in AQPs permeability and are strictly conserved among 11 *poplar* plasmalemmic AQPs (PIPs) (figure 1) while the expression of their genes is differentially regulated during drought.

Molecular dynamics simulations and *E. coli* AQPZ structure hinted another gating mechanism voltage-dependent involving the arginine of the ar/R constriction[15][16][17]. The positively charged guanidinium group of the arginine could act as a sensor of its electrostatic environment oscillating between an up-state, which allows rapid water flux, and a down-state which reduces or interrupts the single-channel water permeability[16]. In this work, we demonstrate by molecular dynamics, that this voltage-dependent gating mechanism could be extended to other AQPs. Interestingly, our results show how distinct AQPs could have different voltage sensitivities. Our calculations allowed us to propose a new method to calculate and better evaluate the permeability coefficient. Altogether, our results coupled to previously published permeability measurements suggest that voltage sensitivity could be a general mechanism in specific AQP isoforms to reduce water loss and dehydration of the cell. These findings pave the way to a general understanding of the molecular features underlying the role of AQPs in the response to environmental stresses.

Materials and Methods

Molecular Dynamics Simulations

All simulations were performed with Gromacs (v.2018.1) [18] in a CHARMM36m force field [19]. The systems were built with CHARMM-GUI interface[20]. A first minimization step was followed by 6 equilibration steps during which restrains applied on the protein backbone and side chains and on lipids were progressively removed before the production phase performed without restrains. Pressure and temperature were kept constant at 1 bar and 303.15 Kelvin respectively using Berendsen method during equilibration and Parrinello-Rahman and Nose-Hoover methods during production. Lennard-Jones interactions threshold was set at 12 angstroms and the long-range electrostatic interactions were calculated through particle mesh Ewald method.

Three experimental setups were carried out:

- First, mimicking J. S. Hub et al. 2010 methods, double membranes of POPC lipids were created with the following AQPs inserted into : *Hs*AQP4 (pdb 3GD8), *Ec*AQPZ (pdb 1RC2), *So*PIP2;1 (pdb 1Z98), *At*TIP2;1 (pdb 5I32) and *Pta*PIP2;1 and *Pta*PIP2;4 (Homology modelling with *So*PIP2;1, with which they share more than 80% of sequence identity, as a template with swiss-model[21]). KCl ions were explicitly used to equilibrate the systems to a zero net charge and to generate a 150mM concentration. From this condition different membrane potential variations were generated: -0.13V, +0.13V, -0.91V and +0.91V (see supplementary figure 1 for more information). Each condition was then simulated during a time course of 30ns.

- Another set of systems was built similarly for *Hs*AQP4, *So*PIP2;1, *Pta*PIP2;1 and *Pta*PIP2;4 insuring KCl ions were distributed as follow. Concentration gradients arose between intra-cellular and extra-cellular compartments *i.e.* : 150mM/150mM, 150mM/600mM and 600mM/150mM. Each condition is then simulated for 30ns as well.

- Finally, *Hs*AQP4, *So*PIP2;1, *Pta*PIP2;1 and *Pta*PIP2;4 were also embedded in a simple POPC bilayer with 150mM of KCl. Mutations of residues of the extra-cellular loops were generated *in silico* : for *Hs*AQP4, asparagine 206 was replaced by an aspartate ; for *So*PIP2;1, glutamate 42 was replaced by a glutamine ; for *Pta*PIP2;1, asparagine 42 was replaced by an aspartate and for *Pta*PIP2;4, aspartate 44 was replaced by an asparagine. Each system was then simulated for 60ns

Analysis

Permeability coefficient (*pf*) was calculated according to the collective coordinate method [22] (see supplementary data for more details). Distances are computed with gmx tool pairdist and water molecules are monitored through the MDAnalysis library[23]. Water free energy profiles were extrapolated from the logarithm function of the counts.

Statistical analysis of *pf*, number of permeation events, mean distances and free energy profiles are performed from 5ns sub-trajectories for each monomer, hence leading for each condition to 24 repetitions (see supplementary data for more details).

Results and discussion

Voltage-gating, clues for a conserved mechanism

The mean *pf* spanning all the conditions for *Hs*AQP4 is equal to $2.17.10^{-14}.cm^{-3}.s^{-1}$ which falls into the range of values obtained by J. S. Hub et al.[16] for the same AQP and comforts the accuracy of the presented results. Figure 2 displays the *pf* as a function of the membrane potential. According to J. S. Hub et al. [16] high membrane potentials (around one order of magnitude higher than in a biological context) can have a significant impact on the permeability of the channel (more precisely on *Hs*AQP1): a positive potential enhancing the *pf* while a negative one would decrease it[16].

This pattern is observed for *Escherichia coli* AQPZ where a significant decrease in *pf* is correlated with a fall of the smallest ar/R constriction distance from ~ 0.3nm to ~0,2nm (figure 2.a.). This value is below the diameter of a water molecule and hence corresponds to a closed state (figure 2.c.). This result is consistent with the literature as AQPZ is the only AQP for which this particular closed conformational state has been observed in a crystal structure[15] (pdb: 2ABM). *E. coli* cell must be able to adapt to multiple environments and is indeed capable to grow in a wide range (at least 100-fold) of osmolarities[24]. It has been shown that bacterial response to hyperosmotic stress depends on the nature of the osmoticum (i.e. ionic or non-ionic): while ionic hyperosmotic stress results in a depolarization of *E. coli* plasma membrane, non-ionic hyperosmotic stress can lead to an hyperpolarization[25]. Water leakage could trigger this hyperpolarization by increasing the concentration of some constitutive intra-cellular negatively charged osmolytes such as proteins and nucleic acids[24], resulting in closed *Ec*AQPZ channels preventing the cell a further water loss. While more investigations need to be carried out to assess the relevance of voltage-gating in a biological context, it is appealing to consider that the arginine of the ar/R constriction in bacterial AQPs may act naturally like a sensor to the osmotic/ionic variations of the environment to prevent directly the stress that would result from leakage of high amount of water from the cell when confronted to hyperosmotic stresses or ultrafast perturbations associated with local ionic transport insured by dedicated membranes transporters.

In contrast, *Hs*AQP4 does not seem to respond to membrane potential fluctuations. Again, this is in good agreement with J. S. Hub et al. 2010[16] as they observed the same tendency as AQP1 for *Hs*AQP4 although not in a significant way. *Hs*AQP4 is one of the main AQPs in the nervous system[26][27][28] and hence it is constantly exposed to fluctuating membrane potentials. A voltage-tolerant AQP in such specialized tissues might be necessary to maintain coherent water fluxes and well-functioning cells.

*So*PIP2;1 and *At*TIP2;1 also display a change of *pf*, although less significant than *Ec*AQPZ, when membrane potential is changed. Therefore, it appears high voltage associated gating seems to be a conserved feature among AQPs as this phenomenon has already been observed in mammal[16] (*Hs*AQP1), bacterial (*Ec*AQPZ, figure 2) and plant (Spinach PIP2;1 and *Arabidopsis thaliana* TIP2;1, figure 2) AQPs simulations. Moreover, these results allow to classify the AQPs depending on their sensitiveness to voltage: high voltage tolerant isoforms (following the example of

*Hs*AQP4), high voltage sensitive isoforms (following the example of *Ec*AQPZ) and intermediate isoforms (following the example of plant AQPs *So*PIP2;1 and *At*TIP2;1) (figure 2.a.). Interestingly, the impact of voltage upon *pf* does not seem to systematically correlate with the diameter of the ar/R constriction. For example, *At*TIP2;1 is an aquaammoniaporin [29] which possesses a wider constriction than strict AQPs, way above the diameter of a water molecule, but it still displays a permeability modulated by the membrane potential (figure 2.a).

Biological relevance: a focus on poplar AQPs

According to these results, three types of potential response to membrane polarity that rely on their sequence diversity could be described. Could this diversity serve a necessity to respond to multiple contrasted situations *in situ* that could explain in part the multiplicity of plant AQPs? To address this question, we simulated, aside of the four AQP structures, two poplar PIP2 obtained by homology modeling.

We used *Populus tremula x alba* PIP2 sequences to build the homology models as this is the reference species for which the genome is sequenced and thoroughly annotated. To choose between all the isoforms, we compared their transcripts abundance in the leaves of trees undergoing drought (supplementary figure 9) and picked the two PIP2 genes with the most contrasted profiles : *Pta*PIP2;1 and *Pta*PIP2;4. Regarding voltage-gating patterns, it is comforting to see that they display different types of response to membrane polarity with *Pta*PIP2;1 behaving similarly to *Hs*AQP4 (high-voltage tolerant isoform) and *Pta*PIP2;4 being closer to *So*PIP2;1 (intermediate isoform) (figure 2.b).

As voltage-gating results from the electrostatic interactions of the ar/R constriction arginine's guanidinium group with its environment[16], we hypothesized that the concentration in ionic osmolytes of the outer or inner compartment could impact as well the aperture of the channel independently of membrane potential. In order to test this hypothesis, we simulated a standard isotonic concentration of 150mM KCl and two ionic stresses concentration gradients of intra-

cellular 150mM / extra-cellular 600mM and intra-cellular 600mM / extra-cellular 150mM KCl for *Hs*AQP4, *So*PIP2;1, *Pta*PIP2;1 and *Pta*PIP2;4 (figure 3). 600mM is close to sea waters ionic concentrations for NaCl and halophytes can handle around 500mM Na^+ concentrations in their leaves[30]. Moreover, drought can lead to a hyper-accumulation of osmolytes, including ions, both in the apoplasm or the cytoplasm of plant cells depending on their coping mechanisms toward ionic and drought stresses[30].

Based on the diversity of responses toward membrane potentials described previously, we compared voltage-tolerant phenotypes against voltage-sensitive phenotypes for the reference structures and the homology models. Thereafter, on figure 3 is displayed the responses toward ionic stress of *Hs*AQP4 and *Pta*PIP2;1 in regards with *So*PIP2;1 and *Pta*PIP2;4 respectively.

We first compared *pf*, however no significant differences were noticeable (table 1). To better assess whether the pore was conducting water or not, we followed the number of water molecules crossing a 5 angströms long section of the channel containing the ar/R constriction site. This method allowed us to estimate the water permeability of each monomer and to discriminate easily closed channels. It is interesting to note that while the way *pf* is computed in molecular dynamics is a good way to estimate how efficiently a channel could convey water, it is still possible to obtain non-zero *pf* values for closed pores. Moreover, the way *pf* is computed according to the collective coordinate method assumes the simulations to be at equilibrium[22] which is not the case for our systems mimicking KCl concentration gradients. Hence we used this simpler and more straightforward approach to compare AQPs together (further discussed in the next section).

It appears clearly that for both reference structures and homology models, voltage tolerant AQPs permeabilities are significantly higher than voltage sensitive isoforms and that this contrast is conserved during stresses (figure 3. a). These differences in permeabilities correlate well with the size of the ar/R constriction with *Hs*AQP4 and *Pta*PIP2;1 constriction diameters always above 0.35nm whereas *So*PIP2;1 and *Pta*PIP2;4 constriction diameters falling generally under this threshold (figure 3. b). These two contrasted phenotypes can be corroborated by the cumulative number of water molecules permeation events, with on one hand linear progressions to be representative of well-functioning monomers while on the other hand a plateau phase to be typical of a closed state (figure 3. c). When the water free-energy profiles are compared, a significantly higher energy barrier in voltage-sensitive isoforms stands out compared to voltage tolerant ones,

especially between *Pta*PIP2;1 and *Pta*PIP2;4 (figure 3. d). This barrier reflects the closed state of the pore induced by the conformational change of 'ar/R arginine' lateral chain. This arginine can be stabilized in such conformational state for several nanoseconds (see movie 1). Hence, the differences in water permeabilities between these AQP isoforms seem to depend, at least partially, on the aperture of the channel at the ar/R constriction site which is determined by the conformational state of the arginine lateral chain. Electrostatic interactions with the 'ar/R arginine' can trigger the closing or the opening of the channel, however, in ionic stress conditions leading to KCl concentration gradients of 450mM, the propensity for these AQPs to be in a rather closed or open state remains unchanged (figure 3).

The differences in water permeability between poplar *Pta*PIP2;1 and *Pta*PIP2;4 highlighted with this approach are in good agreement with *in vivo* permeability assays of *Populus trichocarpa* PIP2 family (table 1), PIP2;1 conducting water twice as much as PIP2;4 [31]. From both, our *in silico* and Secchi et al. *in vivo* approaches, we can distinguish two opposite phenotypes in poplar PIP2 AQPs : highly efficient water channels like *Pta*PIP2;1 and poorly efficient water channels like *Pta*PIP2;4. Moreover, we highlighted the central role of the 'ar/R arginine' in this phenotypic difference and that it seems independent from ionic concentrations close to what can be found in a biological context of hydric stress. Furthermore, we chose to study *Pta*PIP2;1 and *Pta*PIP2;4 in the first place because their transcript levels are very contrasted in poplar leaves undergoing drought (table 2 and supplementary figure 9) which corroborate their contrasted water permeabilities. We also studied their orthologues expression patterns and transcripts tissue localization in *Populus deltoides* leaves of trees undergoing drought[14]: *Pd*PIP2;1 is always up-regulated while *Pd*PIP2;4 is down regulated in well-watered plants and up-regulated during drought (table 2). Interestingly, *Pd*PIP2;4 presents a pronounced transcript abundance in bundle sheath cells[14], a layer of parenchyma cells surrounding the vasculature that isolates it from the rest of leaves tissues.

During drought, it is crucial for plants to minimize water losses from the photosynthetic tissues such as leaves palisade parenchyma. Transpiration is limited by the closing of stomata and the hydrophobic cuticle, nonetheless cells can still suffer a severe dehydration because of the osmolytes and ions concentration in the apoplasm until undergoing cell death[30]. In the bundle sheath cells of poplar undergoing drought, over expression of PIP2;4, poorly conducting water because of its 'ar/R arginine' being predominantly in a closed state, could act as a safety gate by

limiting water leakage toward the dried out vasculature while PIP2;1 would remain open allowing water exchanges between cells of the photosynthetic parenchyma. When plants are re-watered, PIP2;4 is down-regulated again to ease the water exchanges between the vascular bundles and the rest of leaves tissues[14].

Proposal for an energy-based correction to simulated pf to rank AQP permeabilities to water

pf is commonly accepted as the best way to characterize AQPs permeabilities especially as the collective coordinate method has been developed by Zhu et al. to be applied on short equilibrium simulations[22]. In fact, the obtained permeability coefficient falls usually very close to experimentally deduced *pf* as for *Hs*AQP1 : $pf = 7.5\ 10^{-14}.cm^3.s^{-1}$ from simulations[32] and $pf = 5.43\ 10^{-14}.cm^3.s^{-1}$ from experimental measurements[33]. However, in the present study, we observed closed channels with a disrupted water continuum (see movie) that still yielded non-zero *pf* values. This can be explained by the fact that there still is a thermal agitation of water molecules inside the pore.

The collective coordinate method postulates that since the relevant properties of channel water molecules (such as density and order) are considered independent from the external osmotic gradient in a stationary non-equilibrium state and hence very close to the equilibrium state water properties, the diffusion of channel water in an equilibrium state can be used to derive the osmotic permeability coefficient (*pf)* of a channel in a non-equilibrium state [22] . Then we can consider *pf* as a coefficient describing the maximal transport capacity of a channel in an an-isotonic situation derived from the diffusion of water molecules inside this channel in an isotonic equilibrium state. This method is based on the derivative of a collective variable defined as :

$$dn = \Sigma d_{zi}/L$$

with *dz* as the displacement of the water molecules inside the channel along the pore coordinate (the z axis) during a time *dt* and *L* as the length of the considered channel. Hence, it is important to define the channel section (of length *L*) used to compute *dn* as the part of the pore where water

diffusion is the most constrained along the pore coordinate as lateral diffusion is not included in the collective coordinate. In this respect, we defined the channel as a 4 angströms long section of the pore located at the geometrical center of the AQP in the NPA region where water molecules are known to form a very ordered single file continuum[34]. However, sometimes this approach seems to over estimate the *pf* of an AQP because of the thermal agitation of water still occurring in nonetheless closed monomers (see previous section).

It is very relevant to be able to compute *pf* from simulations in order to compare the obtained results with experimental data. However, another simpler and more direct way to quantify the actual permeability of a channel is to count the water molecules crossing the pore. As we know the ar/R constriction constitutes the most stringent part of the channel, we considered a permeation event to occur when a water molecule crossed a 5 angströms channel section including this constriction. Using this method we managed to highlight two contrasted AQP phenotypes (figure 3 and table 1) corroborated by *in vivo* permeability assays, transcript abundance and localization and plant ecophysiology data (see previous section). In an effort to make the *pf* more precise, we introduced a correction constant to accentuate the effect of the ar/R constriction calculated from the free energy profiles as follows :

$$Dk = [\ 2E_0 - E_{arR}\ ] / E_0$$

with *Dk* the unit free correction constant ; E_{arR} the free-energy at the ar/R constriction site and E_0 the free energy corresponding to the highest free-energy barrier in the channel section used to calculate *pf* (see an example in figure 4. c.). E_0 must be smaller than E_{arR} for the correction to be applied. *Dk* integrates the contribution of the ar/R constriction to water diffusion and is comprised between 1 and 0 : when the difference between the two free-energy barriers tends toward 0, *Dk* tends toward 1. On the other hand, the higher the free-energy barrier of the constriction is, the smaller *Dk* is, eventually reaching a limit of the correction when E_{arR} becomes more than twice as high as E_0. In this case, *Dk* becomes negative and is considered as equal to 0. To adjust the *pf*, one has to multiply it by *Dk* :

$$pf_{corrected} = pf \times Dk$$

We tested this approach on our data (table 1) and obtained two divergent groups of AQPs when looking at the ratio between 'high permeability AQP' (*Hs*AQP4 and *Pta*PIP2;1) and 'low permeability AQP' (*So*PIP2;1 and *Pta*PIP2;4) (table 3).

In the first group (*Hs*AQP4 and *So*PIP2;1), the phenotypic diversity highlighted by the counts of water permeation events and the experimental data accessible in the literature (see previous section) is still hided when the correction is applied to *pf* (table 3). In the second group (*Pta*PIP2;1 and *Pta*PIP2;4), the correction of *pf* makes the ratio closer to computational counts and experimental *pf* (table 3). Moreover, the experimental *pf* values discussed in this case (ratio of 1.8 in table 3) originate from the same study and hence from the same experimental design, approach and laboratory, and correspond to AQPs expressed in the same biological context, which makes the comparisons between PIP2;1 and PIP2;4 experimental *pf* [31] more reliable contrarily to *Hs*AQP4 and *So*PIP2;1 which originate from very different organisms and for which the experimental *pf* compared[35][36] were obtained from different laboratories and with different techniques. Put together, these data suggest that the observed differences in terms of water transport between AQPs of group 1 can only be partly explained by the change in pore diameter at the ar/R constriction in opposition with group 2 where the conformational changes of the 'ar/R arginine' seem to play at least a significant part (corroborated by free-energy profiles in figure 3. d.) in the determination of water permeability for these AQPs. As group 2 AQPs are both members of the same poplar species (*Pta*PIP2;1 and *Pta*PIP2;4), the present mechanism of voltage-gating of the AQPs seems pertinent in explaining a part of plant AQP family diversity.

Re-investigation of the relevance of voltage-gating as a response to physiologically relevant membrane potentials.

Based on this newly developed approach to characterize AQPs water permeability (see previous sections), we investigated the impact of biologically relevant membrane potentials (-0.13V and +0.13V), shown so far to have no effect on *pf* [16], on AQPs water permeability (figure 4). As expected, no significant differences between the two conditions were detected when comparing *pf*, except for *Ec*AQZ (figure 4. a. and b.). This is in good agreement with *Hub. et al.*[16] and with our previous analyses as we observed *Ec*AQZ as the most sensitive AQP to voltage. Surprisingly,

the results point toward an increase in *pf* triggered by a negative potential. However when looking at the number of permeation events and corrected *pf*, two results stand out : (i) *Ec*AQPZ in the present conformation (pdb 1RC2) is not functional. Water molecules are still able to fill the pore however the ar/R constriction is never crossed. Conjointly with another molecular dynamics study where the authors had to introduce an additional potential on the 'ar/R arginine' for several nanoseconds to maintain the system in a functional state[11] it could mean for the *Ec*AQPZ structure (pdb 1RC2) to be in a transitional state between a closed and an open conformation. Nevertheless it still indicates a significant impact of voltage on its ar/R constriction (with a massive change in pore aperture, figure 2.a.) even at physiologically relevant membrane potentials. (ii) Significant differences appear for *Pta*PIP2;4, reinforcing the postulate that negative potentials lower the *pf* whereas positive ones increase it. The same tendency is observed for *Pta*PIP2;1, however in a less significant way ($\alpha < 0.1$) (figure 4. b.) which is in good agreement with its high-voltage less sensitive phenotype. Once again, the free-energy profile of *Pta*PIP2;4 illustrates clearly the importance of the ar/R constriction in this change in permeability (figure 4. c.).

Membrane potentials in plants can vary between -80mV and -200mV [37]. During drought, voltage associated signal transduction is known to occur in guard cells, triggering stomatal closure through an ABA-induced hyperpolarization signal transduction, eventually leading to K+ and water efflux from the cell [38][39][40]. However, the changes in membrane potentials involved are far smaller than the ones studied in the present study as a depolarized guard cell membrane potential is close to -41mV while an hyperpolarized guard cell membrane potential would be around -112mV [39]. The AQPs located on guard cells membranes are mainly PIP1 sub-types[41] which display a different charges repartition at their extra-cellular surface than the PIP2 isoforms studied here. Thereafter, it could be that PIP1s or other AQPs react differently to voltage. However, based on the present study, it appears more likely that AQPs water transport capacity is maintained functional at physiological membrane potential fluctuations but a more precise analysis would be needed to better address this question.

To conclude, our new approach allows for a better discrimination of AQPs based on their water transport abilities and questions again the relevance of voltage-sensing in AQPs water transport tuning. Among the isoforms studied, two display a significant impact of biologically relevant

membrane potentials (figure 4), however a question remains: Are these differences an evidence for a new gating-mechanism or for a non-functional side-effect of another necessary feature conservation ? Whatever the response may be, it is intriguing to see that both AQPs highlighted as potentially sensitive to voltage in the present study are expressed in unstable cellular contexts of cells in direct interaction with rapidly changing hydric and osmotic environments (see previous sections).

Structural basis of plant AQPs diversity for water permeability

In order to understand how the observed differences in terms of permeability can be linked to each AQP structure, *in silico* single mutations are performed on *Hs*AQP4, *So*PIP2;1, *Pta*PIP2;1 and *Pta*PIP2;4 (figure 5). We hypothesized that the conformation of the 'ar/R arginine' lateral chain could be modulated by the distribution of charges on the neighboring extra-cellular loops. Following this idea, we managed to concentrate negative charges at the center of the tetramers for *Hs*AQP4 and *Pta*PIP2;1 and did the contrary for *So*PIP2;1 and *Pta*PIP2;4. These changes can be appreciated when looking at the surface electrostatic potentials before and after the mutation (figure 5). When comparing the permeability of the whole tetramers before and after mutation, the expected tendencies are observed. The concentration of negative charges at the center of the tetramer of *Hs*AQP4 and *Pta*PIP2;1 lead to lower water permeabilities while a diminution of negative charges at this location for *So*PIP2;1 and *Pta*PIP2;4 lead to higher permeabilities. These single mutations are sufficient to significantly reverse the phenotypes of all the AQPs studied except for *Pta*PIP2;1. However, the impact of the mutation on the electrostatic potential differs with the considered AQP. From the most impacted to the less impacted, *Hs*AQP4, *Pta*PIP2;4, *So*PIP2;1 and *Pta*PIP2;1 display approximate changes in their potential gradients of -340mV, +250mV, +80mV and -10mV respectively (when compared with their wild type version : supplementary figure 8) in accordance with the significance of their permeability changes (figure 5). These results also corroborate the different responses observed under conditions mimicking realistic membrane potentials (figure 4). Indeed, for *Hs*AQP4, no significant difference was detectable for a potential change of 260mV (-130mV compared to +130mV) but here the induced change by the mutation is stronger (-340mV). This change in gradient potential induced by the single point mutation could then be strong enough to trigger a significant change in permeability through the modification of the 'ar/R arginine' side chain conformation. For *Pta*PIP2;4, a

modification of the membrane potential of 260mV significantly impacted its permeability and is confirmed by the 250mV change induced by the mutation. And finally, for *So*PIP2;1 and *Pta*PIP2;1, the electrostatic potential gradient differences triggered by the mutation are substantially lower than the previously studied 260mV difference and hence tendencies only can be observed. These differences arise probably from the sequence diversity, yielding divergent and AQP-specific allosteric effects among which some are compensatory as for *Pta*PIP2;1 for which an equivalent modification of its intra-cellular electrostatic potential emerged (supplementary figure 8).

Conclusion and perspectives

To conclude, we showed that voltage-gating described by *Hub et al.* at membrane potentials one order of magnitude higher than potentials measured in living cells is a conserved feature among AQPs and that there is a diversity in the response of AQPs toward these membrane potentials. Even though it does not appear relevant to a biological reality, they allowed us to discriminate at least three phenotypic responses among the crystallographic AQP structures simulated : high voltage tolerant isoforms (following the example of *Hs*AQP4, pdb 3GD8), high voltage sensitive isoforms (following the example of *Ec*AQPZ, pdb 1RC2) and intermediate isoforms (following the example of plant AQPs *So*PIP2;1 and *At*TIP2;1, pdb 1Z98 and 5I32 respectively) (figure 2.a.). From this first screening and by using parallel approaches on top of *pf* to characterize AQPs permeabilities to water, we highlighted a putative effect of membrane potentials closer to a physiological context (-0.13V and +0.13V) as well (figure 4) in *Ec*AQPZ and the homology model *Pta*PIP2;4. Further studies have to be carried out to strongly answer the relevance of this gating-mechanism as a new regulation level, however, based on our results in the present study, we can formulate the following hypothesis : *Ec*AQZ being the most sensitive isoform tested to voltage (figure 2 and 4) and the only one for which a structure revealed the corresponding closed state[15] pdb: 2ABM), voltage sensing in AQP might be a functional feature associated with the necessity to cope with rapidly changing hydric cellular environment in micro-organisms such as *Escherichia coli*. It could constitute an ancestral feature lost along the evolutionary process in higher organisms which developed other mechanism to deal with this issue such as mammals while it could have been conserved and even diversified in other living forms subjugated to a restricted spatial exploration of their environment such as plants where a very rapid modulation of their

plasma membranes water permeabilities might constitute a crucial part of their phenotypic plasticity.

To expand the voltage-gating to other biologically relevant contexts, we also simulated several AQPs in systems with KCl concentration gradients of 450mM which is close to what plant cells can experience during drought[30]. When we compared the different AQPs, *pf* did not yield significant differences. However, when we used a simpler approach and compared the amount of water molecules crossing the pore, we managed to highlight different phenotypes with high permeability AQPs (*Hs*AQP4 and *Pta*PIP2;1) and low permeability AQPs (*So*PIP2;1 and *Pta*PIP2;4). These differences where maintained in drought like ionic stresses and correlate well with the size of the main constriction of the pore, monitored through the position of the arginine of this constriction side-chain. Moreover, these differences in terms of permeability are in good agreement with *in vivo* permeability experiments, transcripts abundance profiles and tissue localization of the two poplar AQPs PIP2;1 and PIP2;4 ([14],[31] and supplementary figure 9). In an effort to fill the gap between the traditionally used *pf* and our simpler counting method, we proposed a correction of *pf* based on the free-energy profiles of water inside the pores which yielded coherent results for *Pta*PIP2;1 and *Pta*PIP2;4 (table 1 and 3). This approach allowed us to estimate more precisely the contribution of the ar/R constriction in the observed phenotypic differences which then seems to be secondary between *Hs*AQP4 and *So*PIP2;1. Together with an enhancement of *pf* independent from the size of the pore observed for *At*TIP2;1 (figure 2), these results suggest the existence of another mechanism probably linked to voltage involved in the determination of water permeabilities in AQPs.

Through *in silico* mutations experiments, we demonstrated the role of extra-cellular charged residues in determining the position of the 'ar/R arginine' side-chain and thereafter the permeability of the channel. Interestingly enough, single mutations were sufficient to reverse the phenotypes of *Hs*AQP4, *So*PIP2;1 and *Pta*PIP2;4. In opposition with the regions coding for the ar/R constriction and the D-loop involved in pH-gating, the residues responsible for permeability diversity are highly variable among poplar PIPs (figure 1 and 6). Figure 6 displays the charged residues from which arises the pronounced electrostatic potential at the extra-cellular plaque and hence which are playing potentially a role in determining the aperture of the ar/R constriction. Negatively charged residues, i.e. carboxylates, positioned in the center of the tetramer, in regard

with the ‘ar/R arginine’ seem to play a crucial role in determining its conformation. Indeed, an aspartate at this location corresponds to the mutated positions significantly impacting the permeability of the channel (red box in figure 6. a). Another carboxylate in the same area is conserved among PIP2 sub-family but not in PIP1 sub-family (black box in figure 6. a). On top of the charged residues, several histidines are also located in these variable extra-cellular loops (blue box in figure 6. a). Because of their pKa close to neutrality, histidines constitute pH-sensors that could change the surface electrostatic potential of this region through their protonation and potentially act as switches (as they do in pH-gating of plant AQPs [6]) between high permeability and low permeability channels. Another study revealed a superior impact of the positively charged residues located at the channel entrances on *pf* [42] over the effect of negative ones in the same area. In fact, according to the authors, positively charged residues around the channel mouth would boost *pf* thanks to their dehydration penalty being much smaller than the penalty of negatively charged residues. Hence the positive charge placed ideally contributes to reduce the collective H-bonds lifetime in the single file region [42] . In the present study, we have demonstrated the effect of negatively charged residues located exclusively at the extra-cellular channel entrance on *pf* as they are susceptible to interact remotely with the guanidinium that gates the channel. Therefore these two results do not seem contradictory for several reasons : (i) regarding the charged residues at the channel mouths, if the dehydration penalty was the main cause for *pf* fluctuations, then the introduction of negatively charged residues in this area should impair *pf* in a non neglectable way as well. However that was not the case [42]. (ii) the authors concluded for a rather neglectable effect of carboxylates on *pf*, but they focused on the cytoplasmic entrance to reach their conclusion whereas we have demonstrated the influence of the charged residues of the periplasmic entrance, at the vicinity of the ‘ar/R arginine’. (iii) in our study, we point out the importance of the relative location of the charged residues (regardless of the nature of the charge) with the conserved ‘ar/R arginine’ (i.e. at the center of the tetramer or in the peripheric border) while Horner and his colleagues only focused on the number of charged residues, regardless of their relative position. Still, both studies comfort the role of residues located on the variable extra-cellular loops on the regulation of the channel permeability. Even though more investigations on the impact of these residues on the aperture of the channel are needed, we have already highlighted here a yet unknown phenotypic diversity relevant to the plant realm. In fact, because AQPs play a central role in plant response to hydric stresses, the residues

involved in these changes in the channel permeability are putative targets to consider for drought resistance plant breeding research.

Acknowledgements

We are grateful to Antoine Mahul, David Grimbichler and Nadia Goué of CRRI service (Centre Régional de Ressources Informatiques) for their precious technical support in managing the local calculus resources. This work was performed using HPC resources from GENCI- [TGCC/CINES/IDRIS] (Grant 2019- [DARI A0060710751]) We want to thank Prof. Mikael 'Airborne' Motelica for sharing his access to a 'shelter for scientists in translation' in Orleans what made possible multiple stays for RM. This work was supported by the Ministry of Higher *Education* and *Scientific* research with providing a PhD Fellowship to RM and has been funded by Université Clermont-Auvergne (UCA) I-Site 'Emergence' research program.

Author contributions

RM : Conceptualization, methodology, formal analysis, investigation, modeling and molecular dynamics; made the illustrations and wrote the original draft

BM : Conceptualization, data collection, critical review

PB : Data collection.

JRP : Formal analysis and mathematical formalism, writing & critical review.

SR : Formal analysis, writing & critical review

JSV : Funding acquisition, writing & critical review

AP : Project administration, critical review

PL : Project administration, Funding acquisition, resources, critical review

DA : Conceptualization & supervision, methodology, formal analysis, investigation, modeling and molecular dynamics; made the illustrations and wrote the original draft

Competing interests:

The authors declare no competing interest.

References

1 Preston GM, Carroll TP, Guggino WB & Agre P (1992) Appearance of water channels in Xenopus oocytes expressing red cell CHIP28 protein. *Science* **256**, 385–387.

2 Abascal F, Irisarri I & Zardoya R (2014) Diversity and evolution of membrane intrinsic proteins. *Biochim Biophys Acta - Gen Subj* **1840**, 1468–1481.

3 Yuan D, Li W, Hua Y, King GJ, Xu F & Shi L (2017) Genome-Wide Identification and Characterization of the Aquaporin Gene Family and Transcriptional Responses to Boron Deficiency in Brassica napus. *Front Plant Sci* **8**, 1336.

4 Hub J & de Groot BL (2008) Mechanism of selectivity in aquaporins and aquaglyceroporins. *Proc Natl Acadamy Sci United States Am* **105**, 1198–1203.

5 Wu B & Beitz E (2007) Aquaporins with selectivity for unconventional permeants. *Cell Mol Life Sci* **64**, 2413–2421.

6 Tornroth-Horsefield S, Wang Y, Hedfalk K, Johanson U, Karlsson M, Tajkhorshid E, Neutze R & Kjellbom P (2006) Structural mechanism of plant aquaporin gating. *Nature* **439**, 688–694.

7 Roche JV & Törnroth-Horsefield S (2017) Aquaporin Protein-Protein Interactions. *Int J Mol Sci* **18**, 2255.

8 Jung JS, Preston GM, Smith BL, Guggino WB & Agre P (1994) Molecular structure of the water channel through aquaporin CHIP. The hourglass model. *J Biol Chem* **269**, 14648–14654.

9 de Groot BL & Grubmueller H (2005) The dynamics and energetics of water permeation and proton exclusion in aquaporins. *Curr Opin Struct Biol* **15**, 176–183.

10 Beitz E, Wu B, Holm LM, Schultz JE & Zeuthen T (2006) Point mutations in the aromatic/arginine region in aquaporin 1 allow passage of urea, glycerol, ammonia, and protons. *Proc Natl Acad Sci* **103**, 269–274.

11 Wang Y, Schulten K & Tajkhorshid E (2005) What Makes an Aquaporin a Glycerol Channel? A Comparative Study of AqpZ and GlpF. *Structure* **13**, 1107–1118.

12 Bradshaw HD, Ceulemans R, Davis J & Stettler R (2000) Emerging Model Systems in Plant Biology: Poplar (Populus) as A Model Forest Tree. *J Plant Growth Regul* **19**, 306–313.

13 Lopez D, Bronner G, Brunel N, Auguin D, Bourgerie S, Brignolas F, Carpin S, Tournaire-Roux C, Maurel C, Fumanal B, Martin F, Sakr S, Label P, Julien JL, Gousset-Dupont A & Venisse JS (2012) Insights into Populus XIP aquaporins: Evolutionary expansion, protein functionality, and environmental regulation. *J Exp Bot*.

14 Muries AB, Mom R, Benoit P, Brunel-michac N, Cochard H, Drevet P, Petel G, Badel E, Fumanal B, Gousset-dupont A, Julien J, Label P, Auguin D & Venisse J-S (2019) Aquaporins and water control in drought - stressed poplar leaves: a glimpse into the extraxylem vascular territories. *Environ Exp Bot*.

15 Jiang J, Daniels B V & Fu D (2006) Crystal Structure of AqpZ Tetramer Reveals Two Distinct Arg-189 Conformations Associated with Water Permeation through the Narrowest Constriction of the Water-conducting Channel. *J Biol Chem* **281**, 454–460.

16 Hub JS, Aponte-Santamaría C, Grubmüller H & de Groot BL (2010) Voltage-Regulated Water Flux through Aquaporin Channels In Silico. *Biophys J* **99**, L97--L99.

17 Xin L, Su H, Nielsen CH, Tang C, Torres J & Mu Y (2011) Water permeation dynamics of AqpZ: A tale of two states. *Biochim Biophys Acta - Biomembr* **1808**, 1581–1586.

18 Abraham MJ, Murtola T, Schulz R, Páll S, Smith JC, Hess B & Lindah E (2015) Gromacs: High performance molecular simulations through multi-level parallelism from laptops to supercomputers. *SoftwareX* **1–2**, 19–25.

19 Huang J, Rauscher S, Nawrocki G, Ran T, Feig M, de Groot BL, Grubmuller H & MacKerell ADJ (2017) CHARMM36m: an improved force field for folded and intrinsically disordered proteins. *Nat Methods* **14**, 71–73.

20 Wu EL, Cheng X, Jo S, Rui H, Song KC, Dávila-Contreras EM, Qi Y, Lee J, Monje-Galvan V, Venable RM, Klauda JB & Im W (2014) CHARMM-GUI Membrane Builder toward realistic biological membrane simulations. **35**, 1997–2004.

21 Waterhouse A, Bertoni M, Bienert S, Studer G, Tauriello G, Gumienny R, Heer FT, de Beer TAP, Rempfer C, Bordoli L, Lepore R & Schwede T (2018) SWISS-MODEL: homology modelling of protein structures and complexes. *Nucleic Acids Res* **46**, W296–W303.

22 Zhu F, Tajkhorshid E & Schulten K (2004) Collective Diffusion Model for Water Permeation through Microscopic Channels. *Phys Rev Lett* **93**, 224501.

23 Michaud-Agrawal N, Denning EJ, Woolf TB & Beckstein O (2011) {MDAnalysis}: {A} toolkit for the analysis of molecular dynamics simulations. **32**, 2319–2327.

24 Record MTJ, Courtenay ES, Cayley DS & Guttman HJ (1998) Responses of E. coli to osmotic stress: large changes in amounts of cytoplasmic solutes and water. *Trends Biochem Sci* **23**, 143–148.

25 Shabala L, Bowman J, Brown J, Ross T, McMeekin T & Shabala S (2009) Ion transport and osmotic adjustment in Escherichia coli in response to ionic and non-ionic osmotica. *Environ Microbiol* **11**, 137–148.

26 Rash JE, Yasumura T, Hudson CS, Agre P & Nielsen S (1998) Direct immunogold labeling of aquaporin-4 in square arrays of astrocyte and ependymocyte plasma membranes in rat brain and spinal cord. *Proc Natl Acad Sci U S A* **95**, 11981–11986.

27 Saadoun S, Bell BA, Verkman AS & Papadopoulos MC (2008) Greatly improved neurological outcome after spinal cord compression injury in AQP4-deficient mice. *Brain* **131**, 1087–1098.

28 Day RE, Kitchen P, Owen DS, Bland C, Marshall L, Conner AC, Bill RM & Conner MT (2014) Human aquaporins: Regulators of transcellular water flow. *Biochim Biophys Acta - Gen Subj* **1840**, 1492–1506.

29 Lindahl V, Gourdon P, Andersson M & Hess B (2018) Permeability and ammonia selectivity in aquaporin TIP2;1: linking structure to function. *Sci Rep* **8**, 2995.

30 Flowers TJ & Yeo AR (1986) Ion Relations of Plants Under Drought and Salinity. *Funct Plant Biol* **13**, 75–91.

31 Secchi F, Maciver B, Zeidel ML & Zwieniecki MA (2009) Functional analysis of putative genes encoding the PIP2 water channel subfamily in Populus trichocarpa. **29**, 1467–1477.

32 de Groot BL & Grubmuller H (2001) Water permeation across biological membranes: mechanism and dynamics of aquaporin-1 and GlpF. *Science* **294**, 2353–2357.

33 Engel A & Stahlberg H (2002) Aquaglyceroporins: Channel proteins with a conserved core, multiple functions, and variable surfaces. In *International Review of Cytology* pp. 75–104. Academic Press.

34 Tajkhorshid E, Nollert P, Jensen MØ, Miercke LJW, O'Connell J, Stroud RM & Schulten K (2002) Control of the Selectivity of the Aquaporin Water Channel Family by Global Orientational Tuning. **296**, 525–530.

35 Tong J, Wu Z, Briggs MM, Schulten K & McIntosh TJ (2016) The Water Permeability and Pore Entrance Structure of Aquaporin-4 Depend on Lipid Bilayer Thickness. *Biophys J* **111**, 90–99.

36 Kirscht A, Survery S, Kjellbom P & Johanson U (2016) Increased Permeability of the Aquaporin SoPIP2;1 by Mercury and Mutations in Loop A. **7**.

37 Bhatla SC (2018) Signal Perception and Transduction. In: Plant Physiology, Development and Metabolism. In pp. 729–765. Springer, Singapore.

38 Hamilton DW, Hills A, Kohler B & Blatt MR (2000) Ca2+ channels at the plasma membrane of stomatal guard cells are activated by hyperpolarization and abscisic acid. *Proc Natl Acad Sci U S A* **97**, 4967–4972.

39 Roelfsema MR, Steinmeyer R, Staal M & Hedrich R (2001) Single guard cell recordings in intact plants: light-induced hyperpolarization of the plasma membrane. *Plant J* **26**, 1–13.

40 Zhang J, Jia W, Yang J & Ismail AM (2006) Role of ABA in integrating plant responses to drought and salt stresses. *F Crop Res* **97**, 111—119.

41 Heinen RB, Ye Q & Chaumont F (2009) Role of aquaporins in leaf physiology. *J Exp Bot* **60**, 2971–2985.

42 Horner A, Siligan C, Cornean A & Pohl P (2018) Positively charged residues at the channel mouth boost single-file water flow. *Faraday Discuss* **209**, 55–65.

43 DeLano WL (2002) The PyMOL Molecular Graphics System. *Schrödinger LLC wwwpymolorg* **Version 1.**, http://www.pymol.org.

44 Humphrey W, Dalke A & Schulten K (1996) VMD – Visual Molecular Dynamics. *J Mol Graph* **14**, 33–38.

Figures legends

Figure 1. (a). *Schematic representation of the ar/R constriction* as *seen from the extra-cellular compartment (left part). These four residues are typical of a strict AQP, forming a polar constriction and the narrowest part of the pore. This selectivity filter is strictly conserved among poplar PIPs (right part).* ***(b).*** *Schematic representation of the intracellular D-loop involved in plant pH-gating (left part). Upon protonation of H193, a conformational change closes the intra-cellular entrance of the channel by creating a hydrophobic barrier mediated by the insertion of V194, P195 and L197 into the pore. The new conformation is maintained by hydrogen bonds between R190, D191 and residues of the N terminus*[6]. *Except for V194 which is replaced by another hydrophobic residue in PtaPIP2;1 and PtaPIP2;2, all these residues are strictly conserved among poplar PIPs (right part). All the representations are made from the model PIP structure SoPIP2 (pdb 1Z98) with PyMOL software*[43].

Figure 2. (a). *Boxplots of pf (top charts, in $10^{-14}.cm^{-3}.s^{-1}$) and smallest distances between arginine and the facing residue of the ar/R constriction (bottom charts, in nanometer) for the four AQPs structures. The membrane potential conditions from left to right are the following : -0.13V (in*

black), -0.91V (in gray) and +0.91V (in lighter gray). ***(b).*** *The boxplots of the same conditions for the two homology models of poplar AQPs. Asterisk on boxplots indicate significant differences with the control condition of -0.13V (Tukey post hoc test after one-way analysis of variance or Bonferroni post hoc correction after Wilcoxon test. * : p < 0.05 ; ** : p < 0.005 ; *** : p < 0.0005).* ***(c).*** *Schematic representation of the ar/R constriction of AQPZ in the –0.91V condition.*

Figure 3. *Comparison between voltage tolerant and sensible AQP isoforms in standard (150mM KCl) or ionic-stress conditions (150mM/600mM gradients). In these conditions, the membrane potentials averaged over the whole trajectories are equal to zero. In the upper half, reference structures HsAQP4 (yellow) is compared to SoPIP2 (blue) and in the other half, homology models PtaPIP2;1 (purple) and PtaPIP2;4 (green) are compared to one another.* ***(a).*** *Number of water molecules crossing the ar/R constriction region (along a 0,5 nanometers pore section) during 5ns sub-trajectories (i.e. 24 repetitions per condition).* ***(b).*** *Minimal distance between the arginine and the histidine of the ar/R constriction in nm.* ***(c).*** *Cumulative number of water molecules crossing the ar/R constriction along the whole 30ns trajectories for each 4 monomers of the standard condition (150mM isotonic KCl concentration).* ***(d).*** *free energy profiles of water inside the pore along the z axis in the standard condition. The z coordinates are centered on the center of geometry of the alpha carbons of the asparagines of the two NPA motifs which corresponds to the center of the channel. Dashed lines indicate the position of the ar/R constriction. Asterisk on boxplots indicate significant differences between the two AQPs (Tukey post hoc test after one-way analysis of variance or Bonferroni post hoc correction after Wilcoxon test. * : p < 0.05 ; ** : p < 0.005 ; *** : p < 0.0005).*

Figure 4. (a). Impact of biologically realistic membrane potential (-0.13V in red and 0.13V in blue) on AQPs water permeability. *Boxplots of pf and number of permeation events for the four AQPs structures as a function of membrane potentials.* ***(b).*** *Boxplots of pf and number of permeation events for the two homology models of poplar AQPs. Black lines indicate the pf corrected with Dk constant. Asterisk on boxplots indicate significant differences between the two conditions of membrane potential : -0.13V and +0.13V (Student T-test or Mann-Whitney test depending on the normality and the homoscedasticity of the datasets. * : p < 0.1; * : p < 0.05).* ***(c).*** *Free energy profiles of water inside the pore of PtaPIP2;4 along the z axis for the two*

membrane potential conditions. The z coordinates are centered on the center of geometry of the alpha carbons of the asparagines of the two NPA motifs which corresponds to the center of the channel. Dashed lines indicate the position of the ar/R constriction and the intra-cellular free-energy barrier of the NPA region.

Figure 5. *Structural basis of water permeability for HsAQP4* ***(a)****, SoPIP2* ***(b)****, PtaPIP2;1* ***(c)*** *and PtaPIP2;4* ***(d)****. The high-voltage sensitivity profile is indicated for each isoform (in bold). For HsAQP4 and SoPIP2;1, native isoform is in yellow and mutated one is in blue while for PtaPIP2;1 and PtaPIP2;4, native isoform is in purple and mutated one in green. For each AQP, a visual representation of the surface electrostatic potential is displayed on the upper side of the box. On the bottom right corner stands a schematic representation of one protomer as seen from the extra-cellular compartment with the name of the single mutation. The mutated residues are represented in licorice and colored according to the native/mutated convention mentioned above. On the bottom left corner is the number of water permeations along 5ns sub-trajectories in regard to the minimal distance between the arginine and the histidine of the ar/R constriction. Asterisk on boxplots indicate significant differences with the native isoform (Tukey post hoc test after one-way analysis of variance or Bonferroni post hoc correction after Wilcoxon test. * : p = 0,1 ; * : p < 0.05 ; ** : p < 0.005 ; *** : p < 0.0005).*

Figure 6. (a). *Schematic representation of PtaPIP2;1 and PtaPIP2;4 superposed structures. The charged residues side chains which therefore participate in the surface electrostatic potential of the extra-cellular plaque are represented in sticks (PtaPIP2;1 in purple and PtaPIP2;4 in green). The arginine of the ar/R constriction side chain is also represented in sticks (in gray). The black dotted box surrounds an aspartate existing in both PtaPIP2;1 and PtaPIP2;4 while the red dotted box stands for the aspartate found in PtaPIP2;4 only and corresponds to the mutated position in figure 4. Blue dotted boxes indicate histidines.* ***(b).*** *Alignment of Populus tremula alba PIP1 and PIP2 and SoPIP2;1 zoomed on the three extra-cellular loops.*

Movie 1. Live illustration of the voltage gating mechanism. *Three synchronized views of 10 nanoseconds of trajectory extracted from the SoPIP2;1 simulation. On the left panel is displayed a*

global view of the whole tetramer. On the right panels are displayed two protomers with opposite phenotypes : a functional one implying the 'ar/R arginine' side-chain to be in an open up-state and a non-functional one with the same arginine side-chain in a closed down-state. The backbone is represented as trace and the pore lining residues and the ar/R constriction arginine and histidine are represented as sticks. The water molecules crossing a 5 angströms long pore section of the channel comprising the ar/R constriction are represented as sticks and colored differently for each monomer. "IN" stands for the intra-cellular compartment and "OUT" for the extra-cellular compartment. The movie was produced with VMD software [44].

Tables

AQP	Computational *pf* [10^{-14}.cm^3.s^{-1}]	Computational counts [number of permeation / 5ns]	Corrected *pf* [10^{-14}.cm^3.s^{-1}]	Experimental *pf*
*Hs*AQP4 (pdb : 3gd8)	2.2±0.1	13.5±1	[1.7;2]±0.1	25±2 10^{-14}.cm^3.s^{-1} (Tong et al. 2016)[30]
*So*PIP2;1 (pdb : 1z98)	1.7±0.1	3.9±0.8	[1.2;1.8]±0.1	1.6±0.1 10^{-14}.cm^3.s^{-1} (Kirscht et al. 2016)[31]
PIP2;1	1.5±0.1	12.3±1	1.5±0.1	0.9±0.05 10^{-2}.cm.s^{-1} (Secchi et al. 2009)* [26]
PIP2;4	1.4±0.1	3.5±0.6	[0.7;1.1]±0.07	0.5±0.03 10^{-2}.cm.s^{-1} (Secchi et al. 2009)* [26]

Table 1. *Channel Permeability indicators (pf and number of permeation events) obtained from simulations (control condition of 150mM KCl isotonic concentration) or in vitro/in vivo experiments : mean ± standard error. The corrected pf corresponds to the introduction of a correcting constant in the calculation of pf. The uncertainty of the Dk constant is figured under brackets (PIP2;1 is not corrected as $E_0 > E_{arR}$). The data from Secchi et al., 2009* [26] *are labelled with an asterisk because the values measured are not homogeneous to pf measured in the present study or by Kisch et al.*[31] *and Tong et al.*[30] *(cm.s^{-1} vs cm^3.s^{-1}). This discrepancy is due to*

methodologies employed for the calculations, we thus suggest to use values from Secchi and colleagues for relative comparison of PIP2;1 and PIP2;4.

species	gene	differential expression		tissue localization	source
		well-watered	during drought		
P. deltoides	PIP2-1	+	++	leaf mesophyl	(Muries et al. 2019) [14]
P. deltoides	PIP2-4	-	++	leaf bundle sheet cells	(Muries et al. 2019)[14]
P. tremula alba	PIP2-1	0	--	leaf veins	supplementary figure 3
P. tremula alba	PIP2-4	0	++	leaf veins	supplementary figure 3
P. tremula alba	PIP2-1	0	--	leaf mesophyl	supplementary figure 3
P. tremula alba	PIP2-4	0	++	leaf mesophyl	supplementary figure 3

Table 2. *Differential expression and tissue localization for AQP genes PIP2-1 and PIP2-4 in Populus deltoides and Populus tremula alba.*

	Computational *pf*	Computational counts	Corrected *pf*	Experimental *pf*
HsAQP4 / SoPIP2;1	1.3	3.5	1.3	15.6
PtaPIP2;1 / PtaPIP2;4	1	3.5	1.7	1.8*

Table 3. *Ratio of permeability indicators means between AQPs with high-permeability phenotypes (HsAQP4 and PtaPIP2;1) and AQPs with low-permeability phenotypes (SoPIP2;1 and PtaPIP2;4).*The comparison was made with the experimental Populus trichocarpa values given in Secchi et al.*

Figures

Figure 1

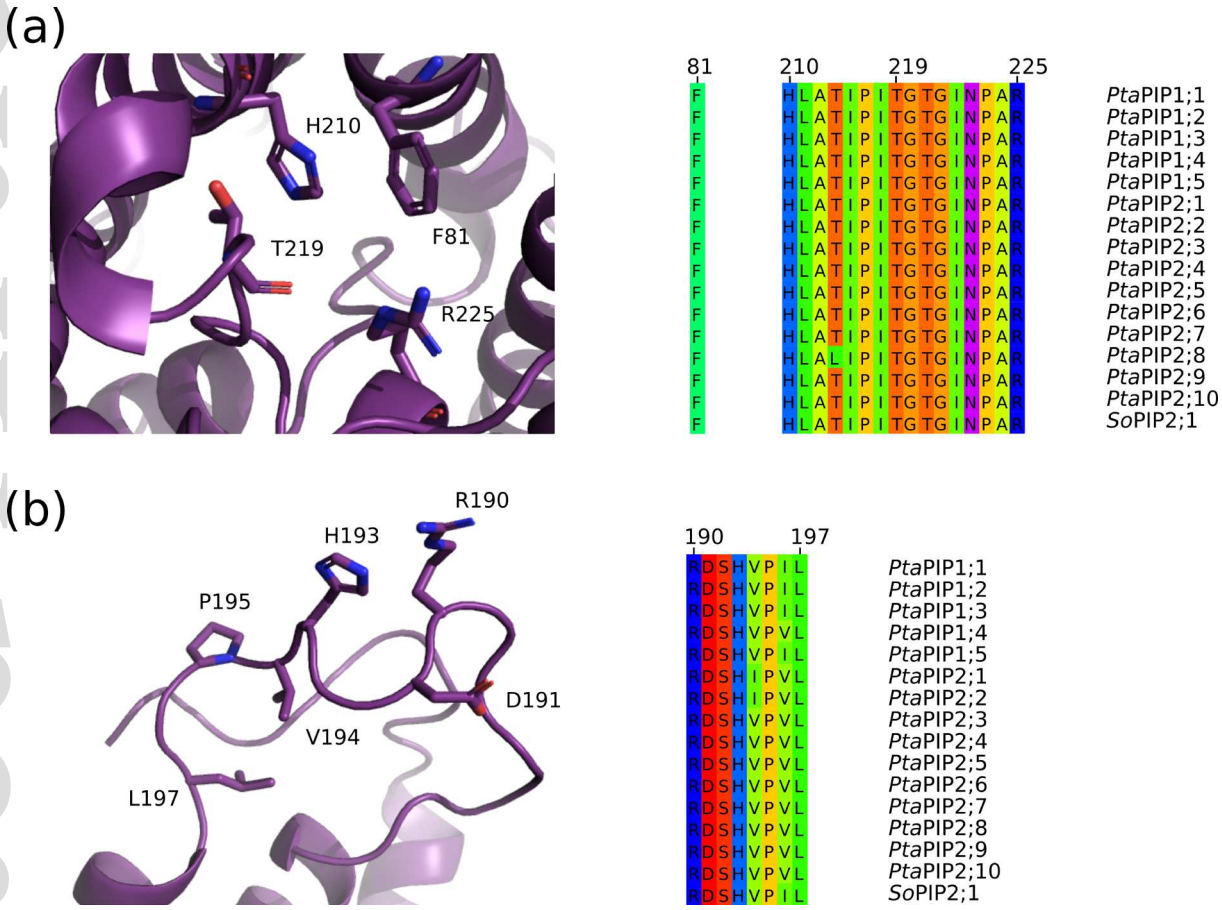

Figure 2

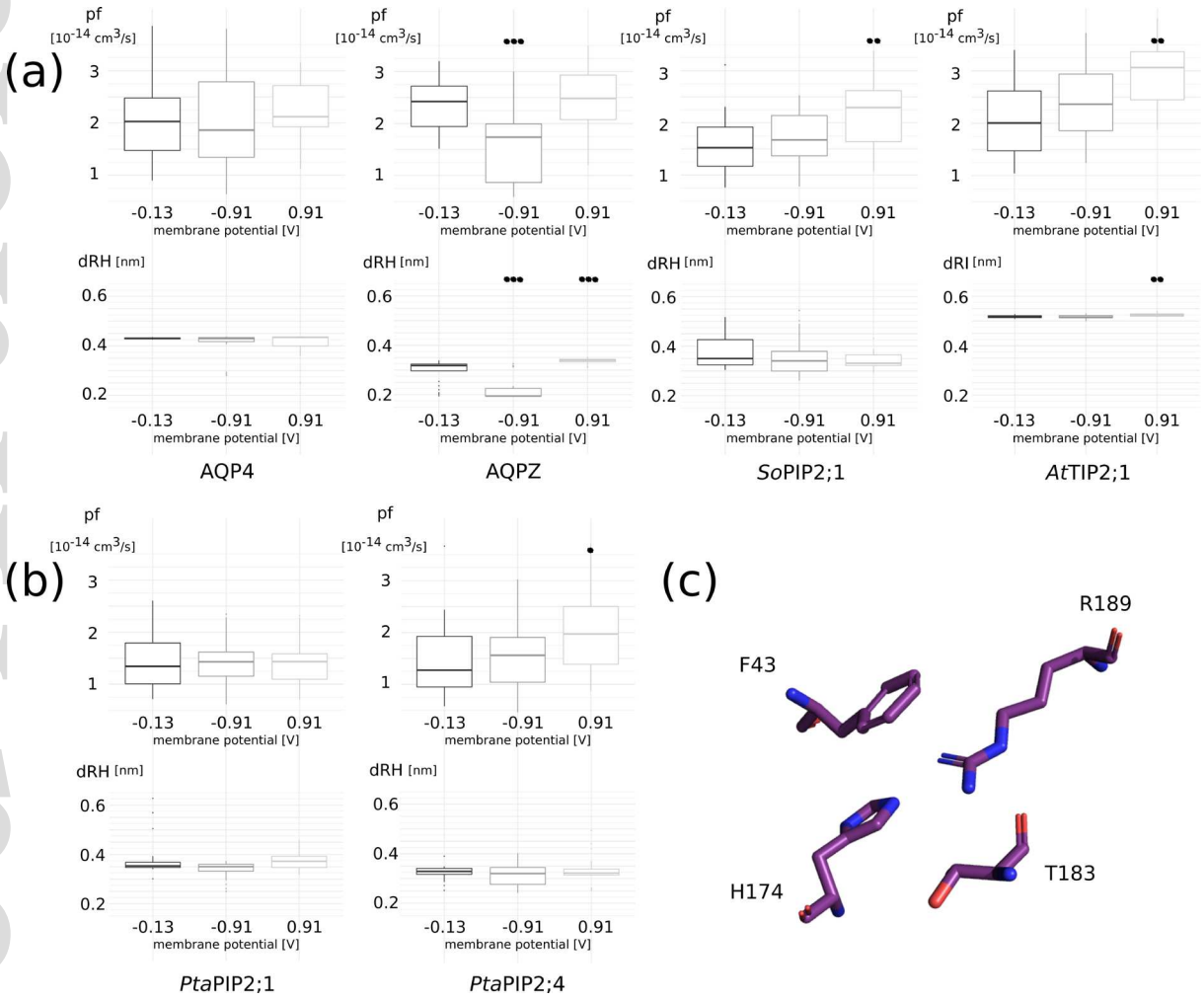

Figure 3

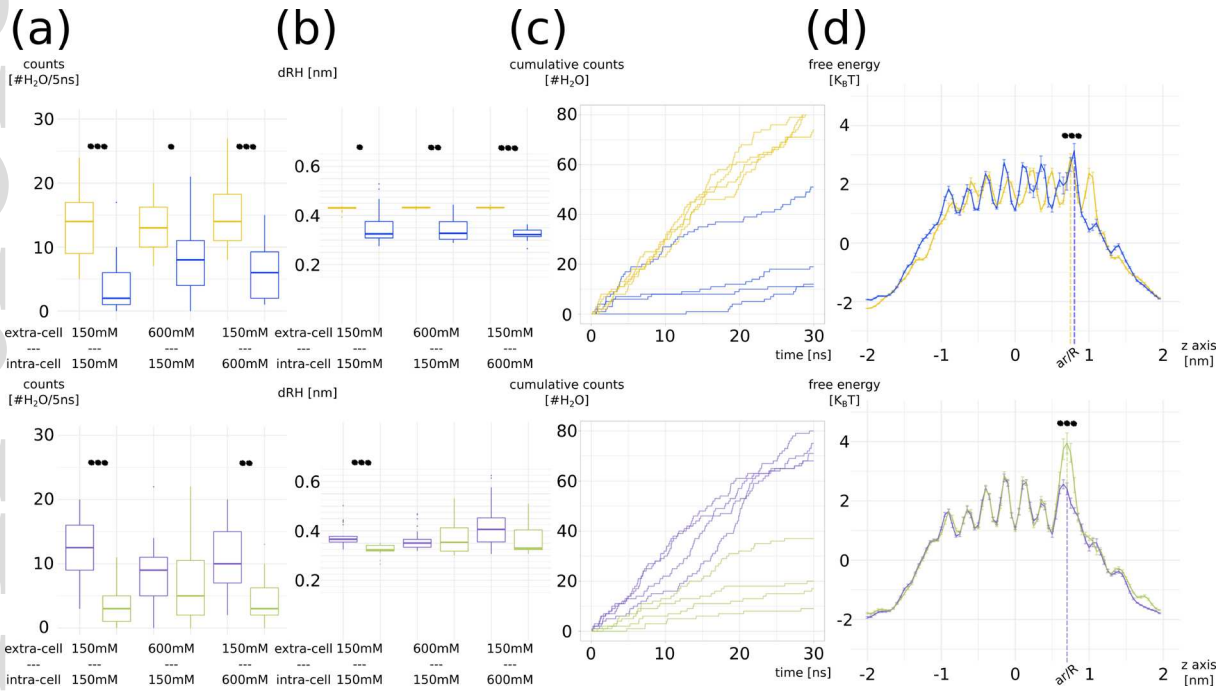

Figure 4

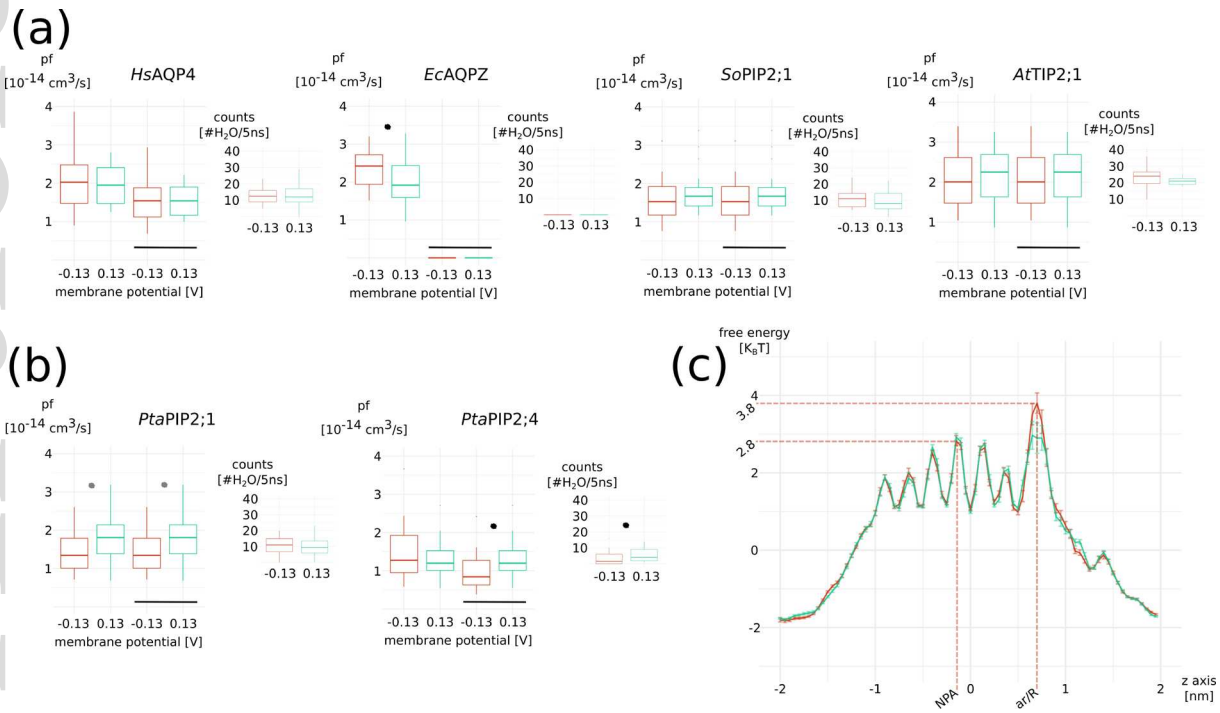

Figure 5

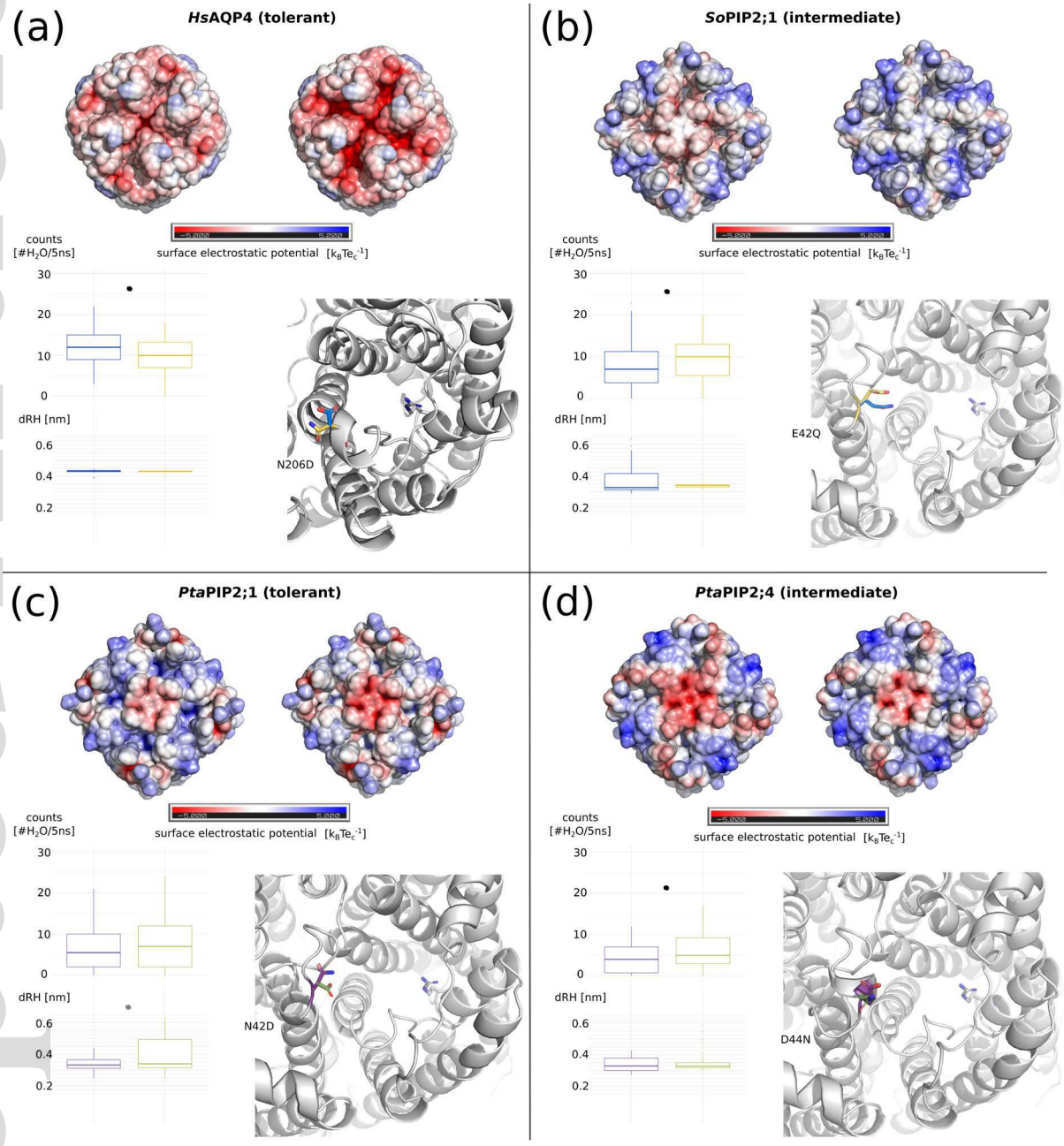

Figure 6

(a)

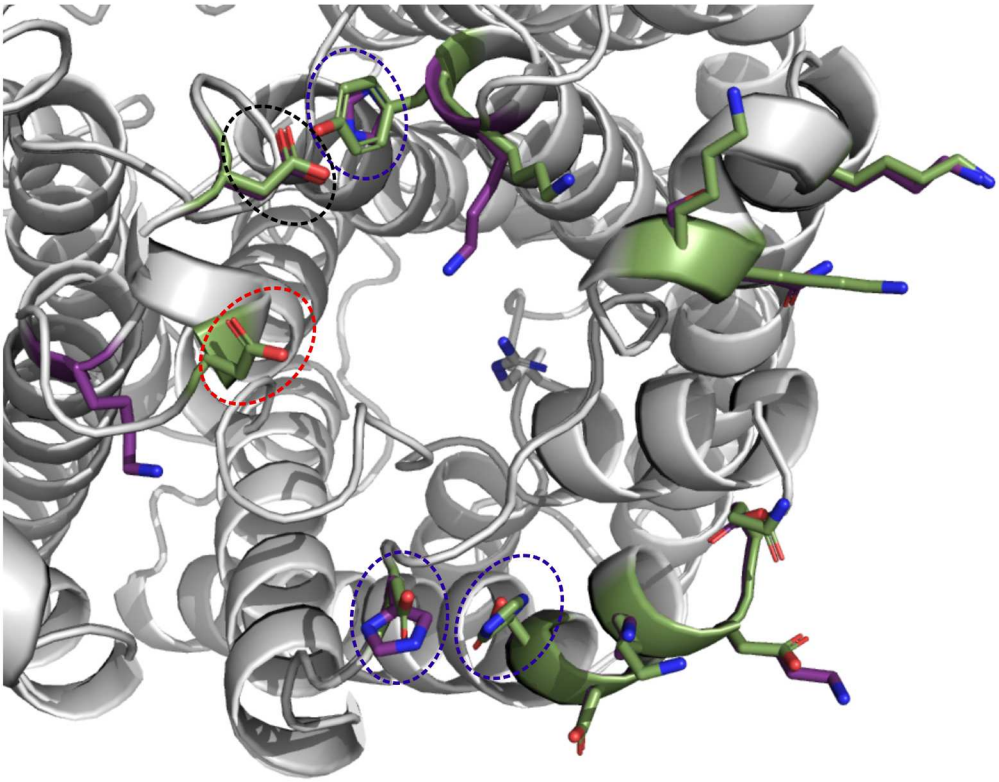

(b)